Microporous and Mesoporous Materials 217 (2015) 190–195

Contents lists available at ScienceDirect

Microporous and Mesoporous Materials

journal homepage: www.elsevier.com/locate/micromeso

HAADF-STEM high-resolution study of nanometric MoS_2 inside mesoporous SBA-15

Maria Girleanu [a, b, *], Susana Lopes Silva [b, c], Dris Ihiawakrim [a], Alexandra Chaumonnot [b], Audrey Bonduelle-Skrzypczak [b], Fréderic Lefebvre [d], Véronique Dufaud [c, d], Anne-Sophie Gay [b], Ovidiu Ersen [a, **]

[a] Institut de Physique et Chimie des Matériaux de Strasbourg, UMR 7504 CNRS-UdS, 23 Rue du Loess BP43, 67034 Strasbourg Cedex 2, France
[b] IFP Energies Nouvelles, Rond-point de l'échangeur de Solaize BP 3, 69360 Solaize, France
[c] Laboratoire de Chimie, UMR 5182 ENS/CNRS, Ecole Normale Supérieure de Lyon, 46 Allée d'Italie, F-69364 Lyon Cedex 07, France
[d] Laboratoire de Chimie, Catalyse, Polymère, Procédés (C2P2), UMR 5265 CNRS, Université Claude Bernard Lyon1, CPE Lyon, 43 Bd du 11 Novembre 1918, 69622 Villeurbanne Cedex, France

ARTICLE INFO

Article history:
Received 19 November 2014
Received in revised form
3 June 2015
Accepted 17 June 2015
Available online 25 June 2015

Keywords:
HAADF-STEM
MoS_2
SBA-15
Heteropolyoxometalates

ABSTRACT

This paper reports on the morphology and the localization of the MoS_2 nanometric phase deposited into a SBA-15 silica network, by means of high angle annular dark field imaging at high resolution into a Cs-corrected scanning transmission electron microscope. Due to the atomic resolution and to the high sensitivity to heavy elements of this incoherent mode, the size, the stacking, the morphology and the precise distribution of MoS_2-based slabs or clusters were precisely characterized. It has been shown that these parameters are strongly dependent on the synthesis method used for the insertion of the sulfide phase precursors, achieved either by direct incorporation of 12-phosphomolybdic acid, $H_3PMo_{12}O_{40}$, into the silica gel using a sol–gel technique or by simple wetness impregnation of this latter in SBA-15 mesoporous silica. The one-pot encapsulation method was found to provide MoS_2 slabs with a better dispersion in the SBA-15 support, comparing to the classical wetness impregnation technique.

1. Introduction

During the last decades, ordered mesoporous materials (OMMs) have attracted a great deal of interest due to their various applications ranging from hosting bioactive molecules [1–3], based on their adsorption [4] and sensing [5] properties, to catalysis [6–8] and more specifically oil refining processes [9,10]. In the catalysis field, their high surface area, their pore organization and size distribution, their good enough mechanical and thermal stabilities in some conditions, the possibility of controlling the location and the size of the active phase are some of the main advantages of the OMMs compared to other more conventional supports [11]. Among the various materials with a porosity in the mesoscopic range, MCM-41 and SBA-15 mesoporous silica are particularly well-suited as catalysts supports due to their open porosity and high accessibility to the uniformly-sized pores. More specifically, SBA-15 supports are characterized by large pore diameters, which can be as large as 10 nm, thus allowing relatively large molecules penetrating the pores with less mass transfer limitation as compared to materials with smaller pore sizes (like MCM-41, e.g.). In addition, SBA-15 type silica possesses relatively thick walls providing additional thermal and hydrothermal stabilities, a key factor in some catalytic processes [12].

One of the main application in the field of functional nanomaterials is the use of these periodic mesostructures as hosting matrix for various types of nanoparticles (metallic, oxide or sulfide) and more recently core-shell nanostructures using either "one pot" synthesis approaches or post-synthesis treatments. Note that when using the former method, the active phase precursors are incorporated during the synthesis of the OMMs materials, hence inducing a better dispersion of the nanoparticles within the matrix and preventing pore blockage due to sintering of large particles [13]. In order to optimize the properties of the resulting composites,

* Corresponding author. Institut de Physique et Chimie des Matériaux de Strasbourg, UMR 7504 CNRS-UdS, 23 Rue du Loess BP43, 67034 Strasbourg Cedex 2, France.
** Corresponding author.
E-mail addresses: girleanu@ipcms.unistra.fr (M. Girleanu), ovidiu.ersen@ipcms.u-strasbg.fr (O. Ersen).

http://dx.doi.org/10.1016/j.micromeso.2015.06.021
1387-1811/

many recent works have been devoted to studying the characteristics and the distribution of particles within OMMs supports [14–19].

Transition metal sulfides supported on alumina, silica or silica-alumina represent a major class of industrial hydrotreating and hydrocracking catalysts, used in oil refining processes [20]. In order to obtain the MoS_2 phase, these catalysts are usually prepared by incipient wetness impregnation of the metal phase precursor (typically ammonium heptamolybdate as Mo source, dissolved in distilled water) over the oxide support (typically γ-alumina), followed by calcination and sulfidation in a H_2S atmosphere [21,22]. The major drawback of the impregnation method lies in the migration of the metallic species and the formation of large metal clusters during the sulfidation step and/or the catalytic reaction. Alternative synthetic approaches have been investigated for the insertion of (W, Mo)S_2 active phases in high surface area mesoporous SBA-15 or related materials [13,21,23]. The benefits of using mesoporous silica support are provided by the presence of a periodically well-controlled porous network and by the ease to put in the practice of the one-pot synthesis method. Among the different preparation routes, one can mention the sonochemical decomposition of metallic (Mo,W) carbonyls in an organic solvent [13,24], or the thermal spreading of active phase precursor [21]. These latter techniques allow the achievement of a better dispersion of the active phase compared to the conventional impregnation. In addition, the functionalization of the mesoporous frameworks by incorporating various ions like Ce, Al, Zr, Ti may improve the acidity and/or increase the density of anchoring sites for the fixation of the active phase [25–28]. However, as a consequence of the surface functionalization, the active phase may also deposit on the external surface of the mesocrystals [11]. To allow a selective deposition of the active phase, within the pore walls, one of the new approaches consists in the direct encapsulation of heteropolyoxometalates, as metal phase precursors, *via* a one-pot synthesis [29,30]. In this case, the simultaneous trapping of the heteropolyoxomatelates during condensation of silica precursors produces relatively stable mesoporous hybrid materials. As shown previously [11,20,24], these systems are active catalysts for the hydrotreating and hydrocracking processes. However, a subsequent optimization of their performances requires a good understanding of the influence of the preparation steps on their microstructural and chemical characteristics. For instance, in addition to the size and the distribution of the active phase, the catalytic performances of these catalysts are also strongly dependent on the localization and the accessibility of the slabs, the number of layers in a slab, the relative amount of the edges compared to the slab core as well as the sulfidation degree.

In order to investigate the structure and the dispersion of the active phase within heterogeneous catalysts as well as its accessibility to the reactions or transformations of interest, several approaches combining electron microscopy and gas adsorption techniques have been developed during the last years. The conventional 2D transmission electron microscopy (TEM) can provide a large variety of information on nanoparticles size and morphology, chemical composition and spatial distribution over a support. In addition to the conventional TEM-based modes, a very useful alternative for analyzing materials at a sub-nanometer scale consists in using a very convergent beam which rasters the sample for acquiring various signals for each position of the beam. This so-called scanning TEM (STEM) illumination mode opens new perspectives for the sub-nanometric analysis of nanomaterials. In particular, by collecting only high-angle scattered electrons with an annular detector, the image intensity is dependent on the atomic number within the specimen and roughly proportional to $Z^{1.7-2}$ [31,32]. A HAADF-STEM (high-angle annular dark field) image is thus characterized by a Z-contrast dependence, and this mode is thus very appropriate for the study of small nanoparticles made of heavy elements, especially if they are deposited on a lighter support. In the last few years, this incoherent imaging mode was extensively used for analyzing the dispersion of metal-based particles within mesoporous supports [33–37]. It should be noted that, in the case of very small nano-objects or for reaching atomic resolution, a probe spherical aberration corrector is required, that provides very small and intense electron probes [38].

In the case of transition metal sulfide slabs deposited on an industrial support such as silica-alumina or γ-alumina or inserted into a mesoporous structure, the characterization tool traditionally used for their analysis is the classical TEM mode [13,21,23,39–42]. It provides first insight and information on some general parameters such as the length and stacking of the slabs. However, it does not allow to precisely solve their shape and structural characteristics. Due to its high sensitivity to heavy metallic atoms (such as Mo, W and even Ni), a HAADF-STEM analysis is the best alternative evaluating these parameters. In addition, compared to the TEM mode, HAADF-STEM can provide direct evidence of the presence of metallic clusters on the support or further information on the very small and poorly crystallized slabs. In the field of hydroprocessing catalysts and to the best of our knowledge, we are aware of only one report related to the use of HAADF-STEM for characterizing SBA-15 supported MoO_3 nanoparticles [43]. However, no information on their precise position inside the porous matrix was provided. Alternative studies dealing with the analysis of a MoS_2 phase dispersion in SBA-15 or zeolite supports by classical TEM or XAFS also appeared in the literature [44–46], but, here again, these techniques were not appropriate for providing information such as the precise location of the MoS_2 slabs within the support.

Herein, we report on the use of high resolution HAADF-STEM for localizing and characterizing a nanometric MoS_2 phase within SBA-15 mesoporous supports obtained by various synthesis methods. Two different preparation routes were considered: i) insertion of the metallic phase over a SBA-15 support using an incipient wetness impregnation technique; ii) encapsulation of the metallic active phase within the SBA-15 silica walls during the oxide synthesis, according to the one-pot method developed by Dufaud et al. [29]. As explained before, this latter method may prevent the sintering of the metallic phase during high temperature treatments (such as calcination and/or sulfidation), by trapping the active phase precursors within the silica framework, thus leading to a better dispersion of the active phase with the generation of potentially more active sites. Indeed, Silva et al. have recently shown that $H_3PMo_{12}O_{40}$ based catalysts prepared by the aforementioned encapsulation method were twice as active as their impregnated counterparts in the hydrogenation of toluene [30]. The authors ascribed this different behavior to stabilization effects and/or stronger interactions between the metal phase and the support for encapsulated catalysts but no structural evidences of a change in the nature of the active sites were provided. Herein, we wish to show that thorough characterization of the sulfide phase by high resolution HAADF-STEM may provide deeper insight into the structural factors leading to the enhanced performance observed by Silva et al..

2. Experimental

2.1. Materials synthesis

A reference MoS_2 on SBA-15 (referred to as Mo/SBA-15-I) material was prepared by an incipient wetness impregnation technique for the insertion of the metallic-based phase. The SBA-15 matrix was synthesized according to the Zhao method [47]. The molybdenum precursor is a Keggin type polyoxometalate, 12-

phosphomolybdic acid, ($H_3PMo_{12}O_{40}$). Two materials were prepared by the encapsulation of the Mo precursor within the SBA-15 silica walls during synthesis, according to the one-pot method [29,30]. The as-synthesized material which contains the structure directing agents (P123 and CTAB) was submitted to a calcination step at 490 °C during 12 h to remove the organic templates, and open the porosity. This material is referred to as Mo@SBA-15-D. At this temperature, the Keggin structure of the molybdenum precursor was partially and/or completely decomposed. Hence, in order to reformulate the decomposed species, the calcined catalyst was further extracted with methanol under reflux conditions using a Soxhlet technique, which also allowed the removal of the non-trapped species. This material is referred to as Mo@SBA-15-D-E. The final Mo loading determined by X-Ray fluorescence is between 10% and 15% for the three specimens [30]. Subsequent sulfidation at 350 °C temperature, under a 15% v/v H_2S/H_2 flow, for 2 h yielded the corresponding sulfided MoS_2–SiO_2 catalysts.

2.2. TEM/STEM, EDX/EELS

The TEM and HAADF-STEM analyses were performed on a JEOL 2100F TEM/STEM microscope, operating at 200 kV and equipped with a Cs probe corrector and a GIF Tridiem energy filter. The limit resolution in HAADF-STEM mode was about 0.11 nm. Before observation, the powders were embedded in an epoxy resin and thin slices (about 30 nm) were cut by ultramicrotomy and transferred onto a copper grid covered by a carbon holey membrane. During recording, the camera focal length used in HAADF was 10 cm, corresponding to inner and outer diameters of the annular detector of about 60 mrad and 160 mrad. No filtering procedure was applied to images.

The TEM-EDX and STEM-EELS/EDX spectra have been recorded on the same Cs-corrected JEOL 2100F for various fragments of MoS_2@SBA-15 samples. The acquisition of STEM EDX and EELS spectra on the S–$L_{2,3}$ edge have been performed simultaneously using the DigiScan routine of Digital Micrograph. The total spectrum was obtained by averaging 70 EELS spectra taken with a 2 s exposure time, using a 2 mm spectrometer aperture and an energy dispersion of 0.1 eV.

3. Results and discussions

Three different catalysts have been studied: the first one was synthesized by the classical incipient wetness impregnation route and will be denoted (Mo/SBA-15-I), while the two others were obtained by the encapsulation approach, directly after the calcination step (Mo@SBA-15-D) and after calcination followed by an additional methanol extraction step (Mo@SBA-15-D-E).

Analyzing HAADF-STEM images acquired on large fields of view (Fig. 1), one can observe that in the case of the Mo/SBA-15-I sample, the MoS_2 dispersion over the SBA-15 support is very heterogeneous: a large area of the support, more precisely inside the mesoporous network, is MoS_2-free, only some adjacent pores located nearby the outer surface of the silica grains contain MoS_2 particles, some being even completely filled with MoS_2 slabs (Fig. 1A insert); for catalytic reactivity concerns, this blocking effect leads to non-accessible active sites or to a lower accessible pores volume. In contrast, the catalysts obtained *via* the one-pot method showed a more homogeneous dispersion of the MoS_2 phase: within a ~800 μm^2 area, representative of the whole catalyst, MoS_2 free pores and MoS_2 filled pores coexist (Fig. 1B and C), a dispersion that is much more appropriate for catalytic applications. At some locations, the MoS_2 phase forms peculiar structures such as large slabs which completely fill the SBA-15 mesopores. To obtain information on the long-range localization of the MoS_2 phase within the SBA-15 support, EDX chemical analysis was systematically performed on several aggregates of each catalyst. The EDX spectra are given in Supporting Information (SI.1) for some representative specimens and their quantification allowed observing that the Mo/Si atomic contain is similar on various grains of the same catalyst. As discussed previously, the homogeneity of the MoS_2 filling is not kept at the microscopic scale (inside a given grain of catalyst), and in addition this parameter is specific to each specimen of the three analyzed catalysts.

For the determination of the structural characteristics and of the localization of MoS_2 within the mesoporous matrix, the incoherent HAADF-STEM imaging mode was systematically applied at higher magnification on several representative fragments of the specimens. Fig. 2 shows typical HAADF-STEM images taken for the three studied samples on fragments with the hexagonal axis of the mesoporous structure either parallel or perpendicular to the electron beam, thus providing direct information on the active phase localization. These images confirm the high organization of the mesoporous SBA-15 matrix for all the samples, that demonstrates a good initial long range ordering of the pores and its preservation after the calcination, extraction (when performed) and sulfidation steps. Note that the calcination step performed on the samples obtained by encapsulation does not seem to affect the structure of the SBA-15 support. Indeed, the pore diameter and the silica wall deduced from direct image measurement or by Fourier transform are rather similar for each sample, about 5.50 ± 0.50 nm for the pore size and 3.50 ± 0.50 nm for the silica wall thickness.

For definitively assigning the bright areas observed in the HAADF-STEM images to the Mo-based phase, EELS and EDX chemical analysis have been simultaneously performed on some typical grains in the STEM mode. The analysis of the EDX and EELS

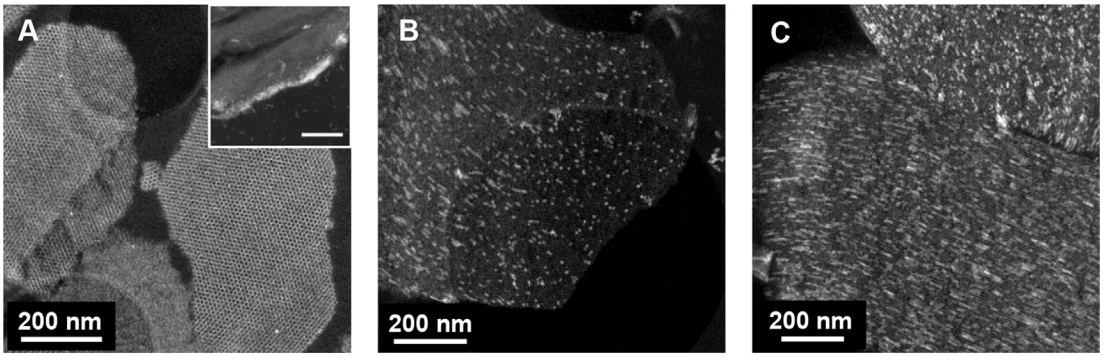

Fig. 1. Typical HAADF-STEM images taken on fragments of the three analyzed catalysts: A) Mo/SBA-15-I; B) Mo@SBA-15-D; C) Mo@SBA-15-D-E. The inset show a HAADF-TEM image of the surface channels of a Mo/SBA-15-I particle completely filled (blocked) with MoS_2 slabs. The scale bar in the insert is 200 nm.

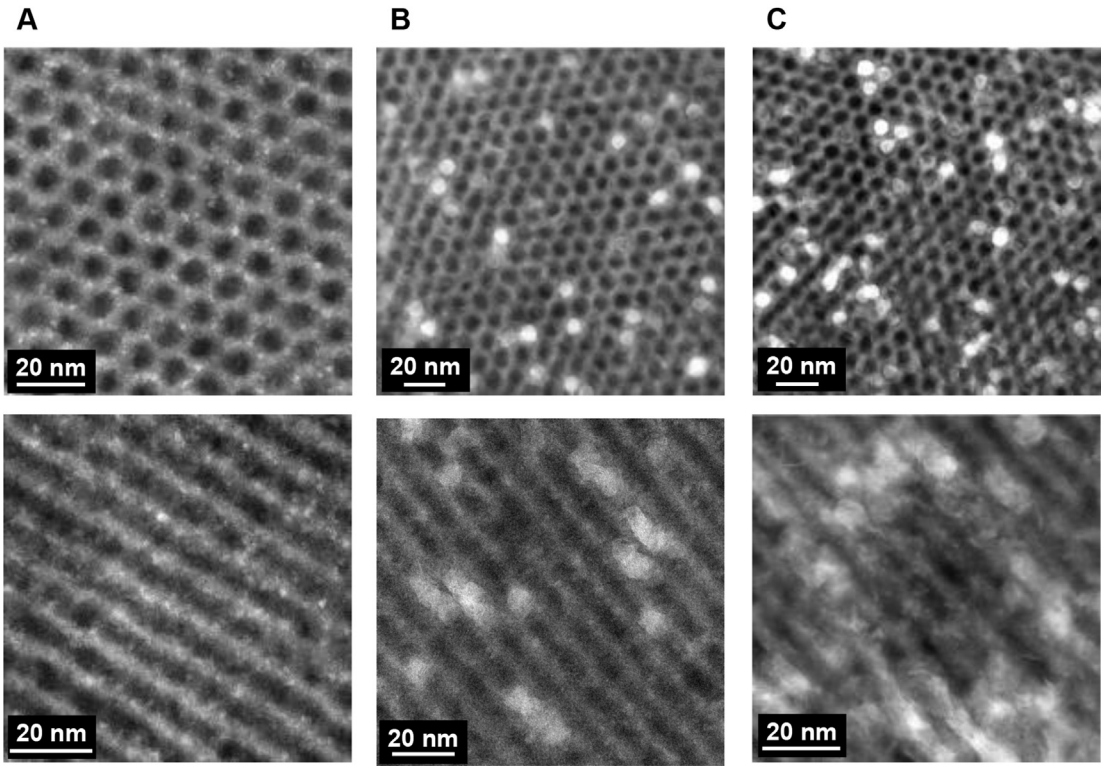

Fig. 2. Typical HAADF-STEM images taken on representative fragments of the MoS_2@SBA-15 samples, parallel (top) and perpendicular (down) to the hexagonal axis of the SBA-15 structure: A) Mo/SBA-15-I; B) Mo@SBA-15-D; C) Mo@SBA-15-D-E.

spectra corresponding to individual small areas surrounding the particles or the slabs (see Supporting Information, SI.2) demonstrates the presence of Mo in the bright areas and of S in the MoS_2 structures with size exceeding about 1 nm. Note that the presence of parallel fringes in the Mo-based particles with a distance of about 6.20 ± 0.50 Å is a clear fingerprint of the formation of the MoS_2 phase. In contrast, the bright areas in the HAADF images with sizes smaller than 1 nm cannot be associated neither to the metallic, oxide, oxy-sulfide phases nor to the metallic sulfide phase at an early stage of formation. On the one hand, there are some experimental drawbacks related to the analysis of such small structures located on or within an oxide matrix, as well as to the potential reductor effect of these structures by the electron beam. On the other hand, from a structural point of view, the MoS_2 phase can be defined only for a minimum of 12 Mo atoms [48–50].

Analyzing the distribution of bright areas over the SBA-15 support, one can observe that for Mo/SBA-15-I, most of the pores are rather free of MoS_2 (Fig. 2A), as observed also before in the low magnification images. However, some small (<1 nm) bright areas can be observed and attributed to the presence of Mo-based clusters in the walls of the mesostructured support. In contrast, the encapsulation method (Fig. 2B and C) leads to the formation of MoS_2 slabs toward the core of the SBA-15 grains. In this case, the MoS_2 structures entirely fill the pore at some locations, forming an aggregate with a cylindrical shape in cross-section and a mean diameter close to the hexagonal pore size (Fig. 2B and C).

Atomic resolution HAADF-STEM images acquired on smaller regions are presented in Fig. 3, for the three analyzed catalysts. As previously observed, small bright areas, attributed to the presence of Mo-based clusters or to small and partially crystallized MoS_2 slabs can be observed once again on the silica matrix for the Mo/SBA-15-I catalyst, Fig. 3A. The previous study reported by Sampieri et al. [21] revealed the presence of MoS_2 slabs partially embedded in the silica walls of the SBA-15 matrix, but they could not conclude firmly on the coexistence of small clusters which are difficult to observe using classical TEM due to the lower resolution and sensitivity of this mode compared to HAADF-STEM. The HAADF-STEM analysis reveals thus that clusters of metal precursor have impregnated the microporosity of the SBA-15. Such a phenomenon was also observed by Yang et al. in the case of Pd deposition [34]. Note that the microstructure and the microporosity of the impregnated Mo/SBA-15-I catalysts do not change drastically compared to that of the SBA-15 support, as deduced by N_2 physisorption [30].

The presence of Mo-based clusters is also observed for the encapsulated catalysts. However, in addition to the small bright areas attributed to the Mo-based clusters or to the weakly crystallized MoS_2 phase, larger and well crystallized MoS_2 slabs are visible on both Mo@SBA-15-D and Mo@SBA-15-D-E images (Fig. 3B and C), when compared to the Mo/SBA-15-I catalyst. Two major morphological types of MoS_2 slabs are observed: i) stacks of 2–3 layered slabs with a length of several nanometers embedded within the silica walls or stuck to the walls; ii) MoS_2 slabs with width close to the pore diameter, that completely fill the mesopores. More precisely, analyzing the image contrast on these slabs, one can also conclude that the MoS_2 structures are not organized as regular slabs, being curved and rather agglomerated to fully fill the available area inside the pores. In addition, a detailed analysis of the longitudinal views of encapsulated catalysts (Fig. 2B and C) shows that some MoS_2 structures that fill the pores are made of several successive individual slabs agglomerated together around the pore centre, giving thus a roughly cylindrical shape for the subsequent MoS_2 aggregates. Note that, from the porosity point of view, additional measurements by nitrogen physisorption performed before the sulfidation step have shown that the specific surface area of the encapsulated specimens undergo a considerable diminution, originating from the introduction of the metallic precursors within the initial structure of the agent micelles, and a loss of the long range

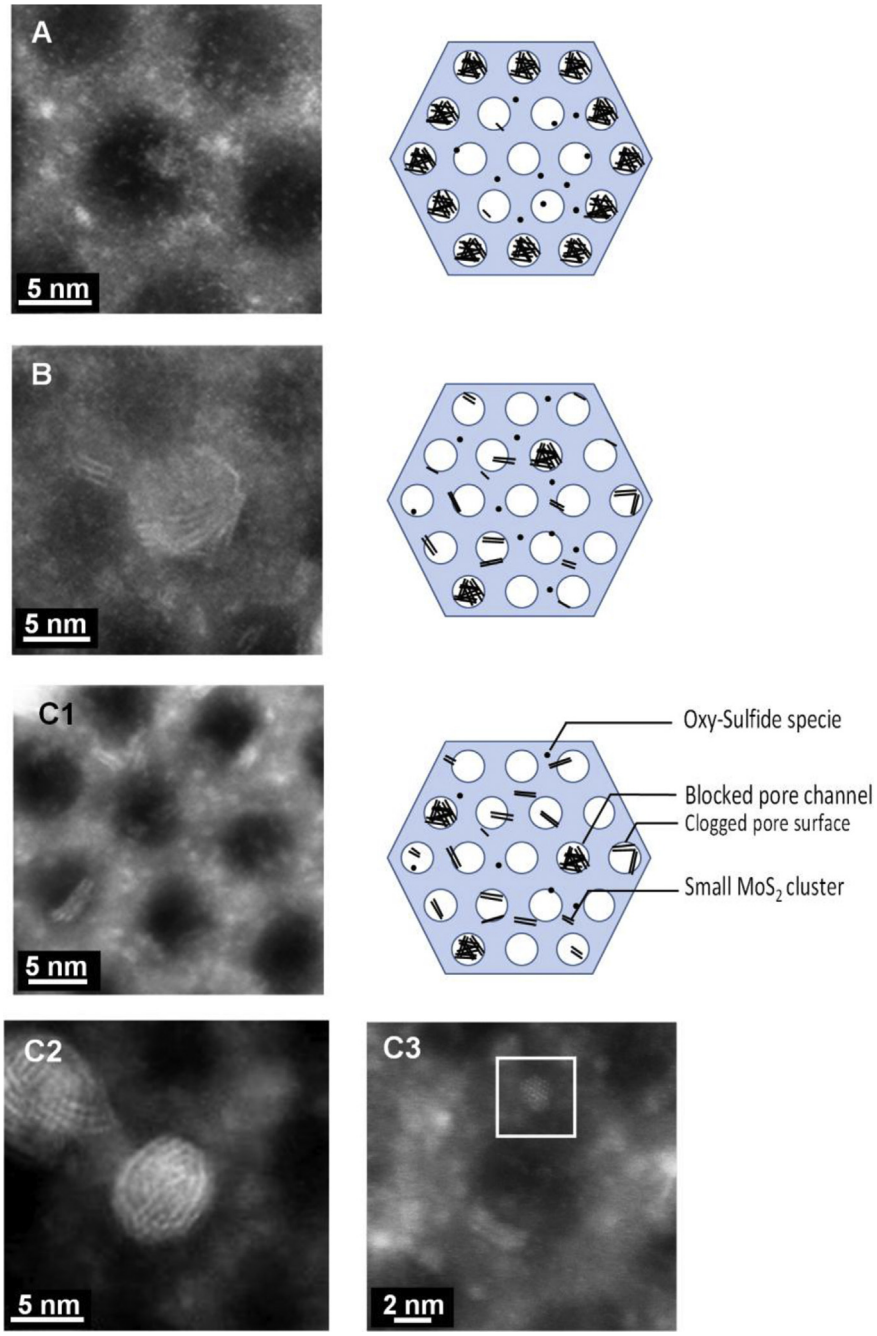

Fig. 3. High resolution HAADF-STEM images for the three investigated catalysts recorded on several representative areas of individual aggregates, parallel to the hexagonal axis of the SBA-15 structure. A) Mo/SBA-15-I; B) Mo@SBA-15-D; C1–3) Mo@SBA-15-D-E. Schematic representations of the MoS_2 phase within the SBA-15 matrix are shown at the right side for the three types of aggregates.

order in the mesoporosity [30]. In addition, as deduced from the same measurements, the extraction step has influenced also the porous characteristics of the initial Mo@SBA-15-D catalyst resulting in a loss of microporosity which can be unambiguously assigned to an atomic level restructuration of the surface.

A more detailed analysis of the Mo@SBA-15-D-E images has revealed the presence in the analyzed grains of some small and curved MoS_2 slabs which do not block entirely the pore, leaving an open entrance in which reactant/product molecules can penetrate (Fig. 3C1). This curved slab morphology involves the existence of some additional sulfur vacancy sites, which leads to an increase in the number of active sites. In addition, a large amount of small and flat MoS_2 slabs can also be observed in this sample. These typical structures have not been observed in the two others samples, for which the HAADF-STEM images were recorded in the same conditions (Fig. 3C3). The presence of a large amount of small and well-crystallized MoS_2 slabs homogenously distributed in the porous network of the SBA-15 matrix is in agreement with a higher catalytic activity of this sample (see Supporting Information SI3), compared to the calcined catalyst which contains mainly small atomic clusters and then less active slabs. This result highlights the major influence of the extraction step (and also the structure of the molybdenum phases before catalyst sulfidation) on the final active phase morphology.

From a general point of view, a considerable improvement of the catalytic performances for the reaction of hydrogenation of toluene was observed in the case of the one-pot encapsulation method compared to the more conventional wetness impregnation technique [30]. The analysis of the results obtained by STEM-HAADF allows assigning the smaller catalytic activity of the impregnated catalyst to the presence of large Mo-based structures close to the surface of the grains which are on the one hand, less active compared to the smaller Mo-based slabs and on the second hand, can block also the accessibility to the inner part of the grains which contains smaller slabs as well. Note that the MoS_2 slabs exhibit a roughly hexagonal morphology (Fig. 3C3, see white rectangle), in good agreement with several models proposed in the literature [49,50] for similar sulfidation conditions. Once again, some subtle morphological differences in the catalyst structure cannot be analyzed using conventional TEM, but do appear using incoherent HAADF-STEM imaging, highlighting the high potential of this latter technique for a sound characterization of sulfided MoS_2-based catalysts.

4. Conclusion

As a conclusion, high-resolution HAADF-STEM imaging was successfully employed to analyze the dispersion of a MoS_2 nanometric phase within SBA-15 mesoporous structures as well as the geometrical and structural characteristics of MoS_2 nanostructures as a function of the synthesis method. Using the classical impregnation method, most of the pores remain generally unfilled, while small metallic clusters were surprisingly well distributed within the pore walls; large MoS_2 slabs are also present close to the external surfaces of the grains. The encapsulation technique leads to a better dispersion of the MoS_2 phase within the whole available volume of the support, inside the mesopores and within the silica walls. The sequential calcination/extraction steps used for the preparation of the Mo@SBA-15-D-E catalyst promotes the formation of small MoS_2 slabs, inside the pores but also within the silica matrix, which leads to a higher catalytic activity and are not generally observed when calcination alone was performed: decomposed Keggin units lead to larger MoS_2 slabs (Mo@SBA-15-D) while intact Keggin structures appeared to have stronger interactions with the silica support, leading to the formation of partially sulfided MoS_2 slabs of hexagonal morphology, under the same sulfidation conditions.

From a general point of view, this study highlights once again the benefit of the HAADF-STEM imaging at atomic resolution for observing and analyzing small and heavy nano-objects and even clusters, deposited on a light support. Such information is crucial for the subsequent understanding and optimization of heterogeneous metallic-based systems, for use in several types of catalytic applications.

Appendix A. Supplementary data

Supplementary data related to this article can be found at http://dx.doi.org/10.1016/j.micromeso.2015.06.021.

References

[1] S.-W. Song, K. Hidajat, S. Kawi, Langmuir 21 (2005) 9568–9575.
[2] M. Vallet-Regi, M. Manzon, J.M. Gonzalez-Calbet, E. Okunishi, Chem. Commun. 46 (2010) 2956–2958.
[3] M. Piras, A. Salis, M. Piludu, D. Steri, M. Monduzzi, Chem. Commun. 47 (2011) 7338–7340.
[4] G.J.A.A. Soler-Illia, C. Sanchez, B. Lebeau, J. Patarin, Chem. Rev. 102 (2002) 4093–4138.
[5] M.E. Davis, Nature 417 (2002) 813–821.
[6] Akira Taguchi, Ferdi Schüth, Microporous Mesoporous Mater. 77 (2005) 1–45.
[7] K. Ariga, A. Vinu, J.P. Hill, T. Mori, Coord. Chem. Rev. 251 (2007) 2562–2591.
[8] L. Yin, J. Liebscher, Chem. Rev. 107 (2007) 133–173.
[9] C.K. Krishnan, T. Hayashi, M. Ogura, Adv. Mater. 20 (2008) 2131–2136.
[10] F. Bataille, J.L. Lemberton, G. Pérot, P. Leyrit, T. Cseri, N. Marchal, S. Kasztelan, Appl. Catal. A General 220 (2001) 191–205.
[11] M.V. Landau, L. Vradman, A. Wolfson, P.M. Rao, M. Herskowitz, C. R. Chim. 8 (2005) 679–691.
[12] D. Zhao, Q. Huo, J. Feng, B.F. Chmelka, G.D. Stucky, J. Am. Chem. Soc. 120 (1998) 6024–6036.
[13] L. Vradman, M.V. Landau, M. Herskowitz, V. Ezersky, M. Talianker, S. Nikitenko, Y. Koltypin, A. Gedanken, J. Catal. 213 (2003) 163–175.
[14] W. Yan, B. Chen, S.M. Mahurin, E.W. Hagaman, S. Dai, S.H. Overbury, J. Phys. Chem. B 108 (2004) 2793–2796.
[15] M.S. Moreno, M. Weyland, P.A. Midgley, J.F. Bengoa, M.V. Cagnoli, N.G. Gallegos, A.M. Alvarez, S.G. Marchetii, Micron 37 (2006) 52–56.
[16] J.A. Melero, J. Iglesias, J.M. Arsuaga, J. Sainz-Pardo, P. de Frutos, S. Blazquez, Appl. Catal. A General 331 (2007) 84–94.
[17] G. Espinosa, J.M. Dominguez, L. Diaz, C. Angeles, Catal. Today 148 (2009) 153–159.
[18] A.B. Laursen, K.T. Højholt, L.F. Lundegaard, S.B. Simonsen, S. Helveg, F. Schüth, M. Paul, J.D. Grunwaldt, S. Kegnæs, C.H. Christensen, K. Egeblad, Angew. Chem. Int. Ed. 49 (2010) 3504–3507.
[19] P. Munnik, M. Wolters, A. Gabrielsson, S.D. Pollington, G. Headdock, J.H. Bitter, P.E. de Jongh, K.P. de Jong, J. Phys. Chem. C 115 (2011) 14698–14706.
[20] H. Topsoe, B.S. Clausen, F.E. Massoth, in: J.R. Anderson, M. Boudart (Eds.), Hydrotreating Catalysis, Springer Series CATALYSIS - Science and Technology, vol. 11, 1996.
[21] A. Sampieri, S. Pronier, J. Blanchard, M. Dreysse, S. Brunet, K. Fajerwerg, C. Louis, G. Pérot, Catal. Today 107–108 (2005) 537–544.
[22] G. Murali Dhar, G.M. Kumaran, M. Kumar, K.S. Rawat, L.D. Sharma, B.D. Raju, K.S. Rama Rao, Catal. Today 99 (2005) 309–314.
[23] L. Dimitrov, R. Palcheva, S. Spojakina, K. Jiratova, J. Porous Mater. 18 (2011) 425–434.
[24] M.V. Landau, L. Vradman, M. Herskowitz, Y. Koltypin, A. Gedanken, J. Catal. 201 (2001) 22–36.
[25] T. Klimova, L. Peña, L. Lizama, C. Salcedo, O.Y. Gutiérrez, Ind. Eng. Chem. Res. 48 (2009) 1126–1133.
[26] J. Zhang, Z. Ma, J. Jiao, H. Yin, W. Yan, E.W. Hagaman, J. Yu, S. Dai, Microporous Mesoporous Mater. 129 (2010) 200–209.
[27] F. Zhang, X. Carrier, J.M. Krafft, Y. Yoshimura, J. Blanchard, New. J. Chem. 34 (2010) 508–516.
[28] S. Badoga, K.C. Mouli, K.K. Soni, A.K. Dalai, J. Adjaye, Appl. Catal. B Env. 125 (2012) 67–84.
[29] V. Dufaud, F. Lefebvre, G.P. Niccolai, M. Aouine, J. Mater. Chem. 19 (2009) 1142–1150.
[30] S. Silva, A. Chaumonnont, A. Bonduelle-Skrzypczak, F. Lefebvre, S. Loridant, V. Dufaud, ChemCatChem 6 (2014) 464–467.
[31] P.D. Nellist, S.J. Pennycook, Science 274 (1996) 413–415.
[32] S. Hillyard, J. Silcox, Untramicroscopy 58 (1995) 6–17.
[33] J.R.A. Sietsma, J.D. Meeldijk, J.P. den Breejen, M. Versluijs-Helder, A.J. van Dillen, P.E. de Jongh, K.P. de Jong, Angew. Chem. Int. Ed. 46 (2007) 4547–4549.
[34] C.M. Yang, H.A. Lin, B. Zibrowius, B. Spliethoff, F. Schüth, S.C. Liou, M.W. Chu, C.H. Chen, Chem. Mater. 19 (2007) 3205–3211.
[35] C.K. Krishnan, K. Nakamura, H. Hirata, M. Ogura, Phys. Chem. Chem. Phys. 12 (2010) 7513–7520.
[36] A.K. Mendina-Mendoza, M.A. Cortés-Jácome, J.A. Toledo-Antonio, C. Angele-Chávez, E. López-Salinas, I. Cuauhtémoc-López, M.C. Barrera, J. Escobar, J. Navarrete, I. Hernández, Appl. Catal. B Env. 106 (2011) 14–25.
[37] X. She, J.H. Kwak, J. Sun, J. Hu, M.Y. Hu, C. Wang, C.H.H. Peden, Y. Wang, ACS Catal. 2 (2012) 1020–1026.
[38] P.D. Nellist, M.F. Chisholm, A.R. Lupini, A. Borisevich, W.H. Sides Jr., S.J. Pennycook, N. Dellby, R. Keyse, O.L. Krivaneck, M.F. Murfitt, Z.S. Szilagyi, J. Phys. Conf. Ser. 26 (2006) 7–12.
[39] R. Nava, R.A. Ortega, G. Alonso, C. Ornelas, B. Pawelec, J.L.G. Fierro, Catal. Today 127 (2007) 70–84.
[40] Z.D. Huang, W. Bensch, L. Kienle, S. Fuentes, G. Alonso, C. Ornelas, Catal. Lett. 124 (2008) 24–33.
[41] P. Rayo, M.S. Rana, J. Ramírez, J. Ancheyta, A. Aguilar-Elguézabal, Catal. Today 130 (2008) 283–291.
[42] Z.D. Huang, W. Bensch, L. Kienle, S. Fuentes, G. Alonso, C. Ornelas, Catal. Lett. 127 (2009) 132–142.
[43] Z. Huang, W. Bensch, W. Siegle, P.A. van Aken, L. Kienle, T. Vitoya, H. Modrow, T. Ressler, J. Mater. Sci. 43 (2008) 244–253.
[44] Y. Okamoto, H. Katsuyama, K. Yoshida, K. Nakai, M. Matsuo, Y. Sakamoto, J. Yu, O. Terasaki, J. Chem. Soc. Faraday Trans. 92 (1996) 4647–4656.
[45] C.-E. Hédoire, E. Cadot, F. Villain, A. Davidson, C. Louis, M. Breysse, Appl. Catal. A General 306 (2006) 1165–1174.
[46] T. Kadono, H. Chatani, T. Kubota, Y. Olamoto, Microporous Mesoporous Mater. 101 (2007) 191–199.
[47] D. Zhao, J. Feng, Q. Huo, N. Melosh, G.H. Fredrickson, B.F. Chmelka, G.D. Stucky, Science 279 (1998) 548–552.
[48] J.V. Lauritsen, S. Helveg, E. Lægsgaard, I. Stensgaard, B.S. Clausen, H. Topsøe, F. Besenbacher, J. Catal. 197 (2001) 1–5.
[49] C. Arrouvel, University of Pierre et Marie Curie, Paris VI, France, 2004.
[50] P. Raybaud, Appl. Catal. A General 322 (2007) 76–91.